A Theoretical and Experimental Study of Positive and Neutral LiF Clusters Produced by Fast Ion Impact on a Polycrystalline LiF Target

F. A. Fernandez-Lima,[†] O. P. VilelaNeto,[‡] A. S. Pimentel,[§] C. R. Ponciano,[∥] M. A. C. Pacheco,[‡] M. A. Chaer Nascimento,[⊥] and E. F. da Silveira*,[∥]

Chemistry Department, Texas A&M University, College Station, TX, Electrical Engineering Department, Pontifícia Universidade Católica, Rio de Janeiro, Brazil, Chemistry Department, Pontifícia Universidade Católica, Rio de Janeiro, Brazil, Physics Department, Pontifícia Universidade Católica, Rio de Janeiro, Brazil, and Chemistry Institute, Universidade Federal do Rio de Janeiro, Rio de Janeiro, Brazil

Received: August 11, 2008; Revised Manuscript Received: December 25, 2008

The positive and neutral clusters produced by the impact of ~60 MeV ^{252}Cf fission fragments on a LiF polycrystalline target are analyzed. The positive ion spectrum is dominated by the $(LiF)_nLi^+$ series, $n = 0-7$, exhibiting a total yield 2 orders of magnitude higher than that of the $(LiF)_n^+$ series. The yield for the dominant $(LiF)_nLi^+$ series decreases roughly as $\exp(-kn)$, where $k \approx 0.9$ for $n = 0-3$ and $k \approx 0.6$ for the heavier clusters ($n = 4-9$), while the yield of the $(LiF)_n^+$ series also decreases exponentially as n increases with $k \approx 0.6$. Theoretical calculations were performed for the $(LiF)_nLi^0$, $(LiF)_nLi^+$, and $(LiF)_n^0$ series for n up to 9. For the smaller clusters the structures first obtained with a genetic algorithm generator were further optimized at the DFT/B3LYP/6-311+G(3df), DFT/B3LYP/LACV3P*, and MP2/LACV3P* levels of theory. An energy criterion is used for a proper taxonomic description of the optimized cluster isomers. Cluster properties such as fragmentation energy and stability are discussed for the proposed configurations. The results show that for all three series the most stable isomers present a linear structure for small cluster size ($n = 1-3$), while cubic cells or polyhedral structures are preferred for larger cluster sizes ($n = 4-9$). Fragmentation energy results suggest that a desorbed excited $(LiF)_nLi^+$ ion preferentially dissociates via a cascade of $(LiF)_n^0$ units, in agreement with the slope modification in the exponential decay of the $(LiF)_nLi^+$ ion abundances for $n \geq 3$.

1. Introduction

The bombardment of alkali (X) halides (Y) by fast projectiles produces a relatively high desorption yield of secondary ions.[1−4] Analyses of secondary ion emission have revealed general features such as: (i) the total yield of positive ions is about 1 order of magnitude larger than that of the negative ions; (ii) $(XY)X^+$ cluster ion yields are 1 or 2 orders of magnitude higher than those of the $(XY)^+$ ions; (iii) mean emission energies are larger for positive than for negative secondary ions.[3−5] On the other hand, many differences among them have been reported, e.g.,: (i) most of the alkali halides, such as NaCl, LiF, LiCl, and LiI, crystallize in the face-centered cubic (fcc) structure with the exception of some cesium salts, namely, CsCl, CsBr, and CsI, that present a body-centered cubic (bcc) crystalline structure;[6] (ii) their molar absorption coefficient range over more than 2 orders of magnitude for UV radiation;[7] (iii) in particular, for ion bombardment of a LiF target, the dependence of the Li^+ and F^- desorption yields on the projectile velocity shows a very different behavior;[3−5] (iv) in-flight fragmentation of $(XY)X^+$ cluster ions depend on their individual properties (e.g., stability, bond length, and charge distribution).[8,9] Cluster properties depend on the size and nature of atomic constituents, i.e., the properties are intimately related to the X and Y constituent electronic densities. Analysis of the cluster properties requires a detailed characterization of each member of the cluster ion series. Some general properties of the alkali halide clusters can be found in the reviews by Johnston[10] and Martin.[11]

From the experimental approach, two techniques have been previously used to produce charged species out of a LiF target: (i) laser ablation and (ii) fast projectile impact. Since LiF is transparent to visible and near UV light, absorbent materials such as Li_3N were mixed with LiF powder previous to the laser ablation,[12] and a $(LiF)_nLi^+$ series with n up to 8 was observed after irradiation. Fast projectiles have been used by Itoh et al.,[1] Szymonski et al.,[2] Jalowy et al.,[13] and Pereira et al.,[14] but only the Li_2^+, $(LiF)Li^+$, and $(LiF)_2Li^+$ ionic species were observed. As will be shown in this paper, the combination of heavy ion projectiles (^{252}Cf fission fragments at ~60 MeV) and an adequate time-of-flight (TOF) analyzer allows the identification of larger $(LiF)_nLi^+$ cluster ions, i.e., species having n up to 7.

Theoretical calculations can be very useful in predicting atomic and molecular properties or parameters which might be of difficult experimental verification such as binding energies, ionization potentials, vibration frequencies, and fragmentation patterns of atomic and molecular clusters. They can also be helpful in the interpretation of experiments by providing details of the geometrical configurations and of the electronic density distribution. The structure of LiF chains[15] and of LiF clusters have been analyzed theoretically at different levels,[16−21] e.g., ab initio calculations using the Hartree−Fock method,[18,19] a perturbed ion model,[20] and density functional theory (DFT).[12,21] In particular, the three-atom member structure, $(LiF)Li^+$, was predicted to be linear.[16,17] Aguado et al. have found that the

* To whom correspondence should be addressed. Phone: 55-21-35271272. Fax: 55-21-35271040. E-mail: enio@vdg.fis.puc-rio.br.
[†] Texas A&M University.
[‡] Electrical Engineering Department, Pontifícia Universidade Católica.
[§] Chemistry Department, Pontifícia Universidade Católica.
[∥] Physics Department, Pontifícia Universidade Católica.
[⊥] Universidade Federal do Rio de Janeiro.

10.1021/jp8071684 CCC: $40.75
Published on Web 02/10/2009

magic numbers for all alkali halides are $n = 4$, 6, and 9 independently of the specific ground-state geometry.[20] Yokoyama et al.[12] and Haketa et al.,[21] using DFT calculations, proposed several structures for the $(LiF)_nLi^0$ and $(LiF)_nLi^+$ clusters, $n = 1-4$, and remarked that $(LiF)Li^0$ stability is achieved either for the F nucleus in between the two Li nuclei or in one extremity of the molecule, while for larger structures ($n > 2$) the odd electron is always localized.

The search for small clusters geometries strongly depends on the initial guess structure regardless of the theoretical method. Over the last years, genetic algorithms (GA) have been proposed to improve the number of candidate structures.[22−27] The use of GAs for optimizing cluster geometries was first used in the early 1990s by Hartke et al.[24] and Xiao and Williams[25] for small silicon and molecular clusters, respectively. With the introduction of real-valued genes by Zeiri et al.,[26] the representation of the cluster in terms of continuous variables became possible. Deaven and Ho[27] showed that performing a gradient driven local minimization of the cluster energy after the generation of each new cluster greatly simplifies the energy surface and facilitates the search for the global minimum. In the same work, they introduced a new 3-dimensional crossover operator, called cut and splice, which gives a better physical meaning to the crossover process. Studies on cluster structure optimization have been also performed using GA techniques coupled to molecular mechanics methods.[24−27] Later on, Alexandrova et al. have developed the gradient embedded genetic algorithm (GEGA) technique coupled to ab initio methods which has been used to perform a search for global minima of small cationic, anionic, and uncharged clusters of lithium Li_n ($n = 5-7$)[28] and of sodium chloride anionic clusters, $(NaCl)_nCl^-$.[29] However, the geometry optimization of clusters containing Li and F atoms using GA has not been yet described in the literature.

In this article, we focus the attention on experimental data of charged species emitted from a LiF target by fast ion bombardment and to predictions based on DFT results for the $(LiF)_nLi^0$, $(LiF)_nLi^+$, and $(LiF)_n{}^0$ series. Candidate structures for the $(LiF)_nLi^0$, $(LiF)_nLi^+$, and $(LiF)_n{}^0$ series are obtained out of a pool of "potential" candidate structures generated by a genetic algorithm, which are further optimized at the DFT/B3LYP/6-311+G(3df), DFT/B3LYP/LACV3P*, and MP2/LACV3P* levels of theory. An energy criterion (D plot methodology[30,31]) is employed for a taxonomic description of the cluster isomers. Fragmentation energies, charge distributions, and relative stabilities are reported for the $(LiF)_nLi^0$, $(LiF)_nLi^+$, and $(LiF)_n{}^0$ series with $n = 0-9$.

2. Experimental Approach

Plasma desorption mass spectrometry (PDMS) was used to study the secondary positive ions emitted from a polycrystalline LiF target when bombarded by ~60 MeV ^{252}Cf fission fragments (FF). Details of this technique and of the mass spectrometer are described elsewhere.[8,9] Briefly, a thin film of ^{252}Cf confined between two thin metal foils continuously emits pairs of ^{252}Cf FF; one of these fragments is detected by a microchannel plane detector (MCP) used as a start detector, while the second one traverses an Al thin foil onto which LiF was evaporated in vacuum. LiF cluster ions are produced when the ^{252}Cf FF emerge from the target. The desorbed ions are then accelerated by the extraction field toward the drift region and are detected by a second MCP, used as a stop detector. Signals from both detectors are used in a digital clock for determining the TOF of individual secondary ions.

The extraction potential was 6 kV, and the residual gas pressure was about 10^{-6} mbar. Besides the peaks related to the Li or F species, other peaks due to surface adsorbed molecules are observed in the mass spectrum, such as hydrogen cluster ions (H^+, H_2^+ and H_3^+) and pump oil fragment ions (e.g., m/z of 27, 57, 73, 105, and 147 u). The broad structures or peak tails at the right side of each high peak are mainly due to cluster ion fragmentation in the acceleration region of the TOF spectrometer.[9]

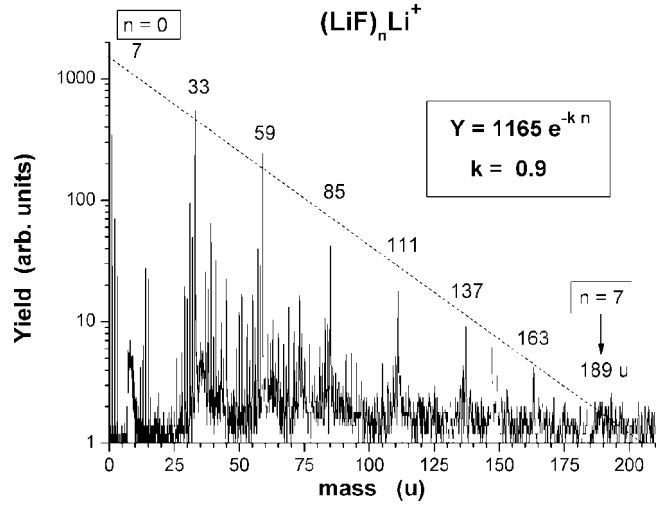

Figure 1. PDMS-TOF spectrum of a polycrystalline LiF target. The $(LiF)_nLi^+$ peaks are predominant. The yields of the $n \geq 8$ species are comparable to that of background.

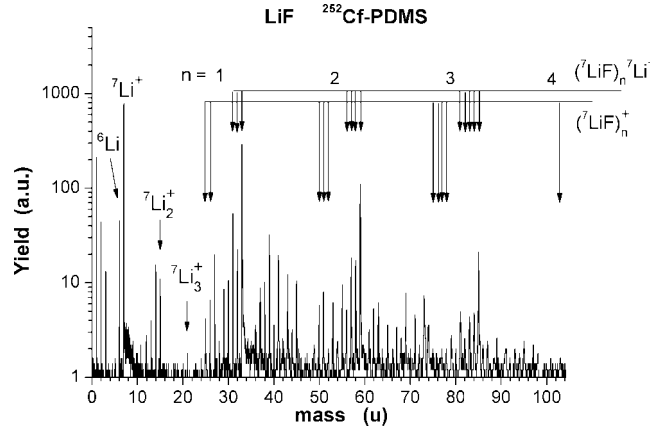

Figure 2. The same spectrum of Figure 1 expanded into the $m = 100$ u range. The Li_n^+, $(LiF)_n^+$, and $(LiF)_nLi^+$ series are identified. Some peaks are due to target surface contaminants.

3. Experimental Results

A typical PDMS-TOF spectrum of a LiF polycrystalline target is shown in Figure 1. More than 50% of the observed positive ions belong to the $(LiF)_nLi^+$ cluster ion series, whose yield distribution shows an approximately decreasing exponential behavior with the cluster number of constituents, n. Ions of the $(LiF)_n^+$ series are also observed and are better visualized in the expanded spectrum of Figure 2. Since the total desorption yield of the $(LiF)_n^+$ series is about 60 times lower than that of the $(LiF)_nLi^+$ series and comparable to those of the contaminant species, the relative desorption yields presented in this work should be taken as their maximum values. Peaks corresponding to m/z of 14 and 21 are attributed to Li_2^+ and Li_3^+, respectively, and form the short metallic $(Li)_nLi^+$ series, the $n = 0$ member being common to both the $(LiF)_nLi^+$ and $(Li)_nLi^+$ series. The double-charged Li^{2+} ion has a very low yield, and its TOF signal

TABLE 1: $(LiF)_n^+$, $(LiF)_nLi^+$, and Li_nLi^+ Relative Desorption Yields[a]

n	0	1	2	3	4	5	6	7	Total
$(LiF)_n^+$		83	82	35	19	19			238
$(LiF)_nLi^+$	8014	3583	1709	410	216	114	61	40	14120
Li_nLi^+	8014	180	15						8209

[a] The Li^+ member is the band head of both $(LiF)_nLi^+$ and Li_nLi^+ series. In all the current calculations, only isotope ^7Li has been considered.

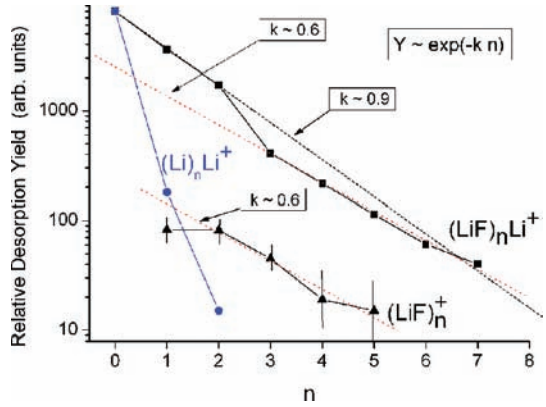

Figure 3. Relative desorption yields for the three desorbed ion series. Experimental data are approximately fitted by exponential functions. The decreasing constant is $k \approx 0.9$ for the $(LiF)_nLi^+$ series and $k \approx 0.6$ for the $(LiF)_n^+$ series and for the heavier $(LiF)_nLi^+$ members.

appears at the background level. Also noticeable in this spectrum is the presence of peaks due to ^6Li and ^7Li ions, whose yields occur in the proportion 1:16, not very different from their expected natural isotopic abundances of 7.5 and 92.5%, respectively. Note that each $(LiF)_nLi^+$ member is formed by $n + 2$ peaks, according to the random occurrence of the two Li isotopes. For the yield calculations reported in Table 1 only the peaks corresponding to the more abundant ^7Li isotope were taken into account.

The relative yields of $(LiF)_n^+$, $(LiF)_nLi^+$, and Li_n^+ cluster ion series are shown in Figure 3 and Table 1. Inspection of Table 1 reveals that: (i) the $(LiF)_nLi^+$ series is the dominant one, and the yield decreases roughly as $\exp(-kn)$, where $k \approx 0.9$ for $n = 0-3$ and $k \approx 0.6$ for the heavier clusters, $n = 4-9$; (ii) the yield of the $(LiF)_n^+$ series decreases as n increases and the data can be also fitted to an exponential function with $k \approx 0.6$; (iii) the Li_n^+ series has only three members and decreases steeply with a $k \approx 3.8$ (considering only the first two members). In the event of some contribution of CH_2^+ ions to the peak of mass 14 u, the Li_2^+ desorbed yield would be lower and the exponential distribution steeper (i.e., a larger k value) than the one reported.

4. Theoretical and Computational Approach

Theoretical calculations were performed for the $(LiF)_nLi^0$, $(LiF)_nLi^+$, and $(LiF)_n^0$ series. A GA was used to account for the higher number of potential isomers as the cluster size increases. An automatic search for cluster configurations was employed based on an algorithm developed for simulation of genetic evolution. However, because of the long computational time, the search for structures using the genetic algorithm was only performed for clusters with n up to 4. For larger clusters ($n > 4$), the search was directed to specific clusters series using DFT and MP2 calculations.

4.1. Search for Stable Configurations: the Genetic Algorithm. Genetic Algorithm (GA) is an optimization and search technique based on the principle of natural evolution.[22] The GA does not include the calculations of derivatives and has been successfully used in many areas of science and technology.[23] Details of previous implementations of GA can be found elsewhere.[23−29]

Briefly, the search for the global minimum using a GA is performed in the 3N configurational space with the energy value as a criterion of fitness. The individuals of the initial population are randomly generated, where the minimum interatomic distance and the maximum cluster volume are defined by the user as a function of the cluster size.

To achieve global geometry optimization of the cluster structures we used the GEGA, proposed by Alexandrova et al.[28,29] For the individuals fitness evaluation the energy was calculated using the DFT/B3LYP method with the 3-21G basis set. All individuals are optimized to the nearest stationary point using the GAUSSIAN 03 software,[32] and the atoms coordinates are updated. All different isomers generated by the GA are stored in a "pool" of candidates. Preliminary experiments showed that the GA search can easily find the global minimum even if some individuals are not true local minimum. As it will be described later, the frequency calculation to check if the stationary points found are true minimum was only realized after the GA run.

In each GA loop, a set of new individuals is created to replace the worst individuals of the population. The percentage of individuals replaced is called GAP. For a consequent reproduction, each individual in the current population is assigned a certain probability to be chosen as a genitor according to its fitness. There are two main genetic operators responsible to create the new individuals: mutation and crossover. Crossover is the process through which the genetic information from two parent chromosome is combined to generate the new individuals. The variation of the cut and splice operator proposed by Deaven et al.[27] has been used. Despite the good performance obtained by this operator, for clusters that present more than one type of element or isomer, it may be hard to find a good position to cut the clusters for generating new individuals with the same number of elements as their parents. To solve this problem, we introduced a mechanism inspired in an order-based crossover,[22] which always generates clusters with the correct number of elements, as described below.

In the proposed crossover, each atom of the two different parents selected has an associated number. First, an orientation axis is randomly chosen among x, y, and z. Next, the atoms on each cluster are sorted with respect to this axis, from higher to lower coordinate points. In this case, the clusters are not cut by a plane, as in the crossover proposed by Deaven et al.,[27] but a cut point is chosen randomly in the selected axis, such as in a binary representation genetic algorithm.[22] The first offspring is formed by the upper or lower part (randomly selected) of the first parent. The remaining atoms are positioned as they appear on the second parent. The second offspring is formed in the same way but by changing the parents. The proposed crossover operator always generates clusters with the correct number of elements.

To avoid stagnation and to maintain population diversity, a mutation operator was used. The mutation perturbs some of the atoms within the cluster. The cluster is mutated by replacing the atomic coordinates of a certain number of atoms with random values. This is done in two different ways. In the first one, the atomic coordinates of some atoms are changed inside a sphere with defined radius around the atom. In this case the operator shifts the atomic coordinates. The radius of the sphere has to be selected by the user as it may differ for each system

being optimized. In the second way, the coordinates are randomly changed in the whole space used. It is known that the mutation operator completely changes small structures such as the ones studied in this work. However, the global geometry of small clusters is not so difficult to be found (normally on the first generations), and the operator was used to generate different local minima and maintain diversity. For any mutation process the interatomic distance has to be evaluated to avoid two atoms getting closer to each other. We have used a mutation rate of 34%, similar to that used previously.[28,29] Normally, a much lower mutation rate is recommended, but since in this case the mutant individuals are locally optimized, a higher rate value was set to avoid convergence of the new individuals to the same local minimum of the parent.

To start the GA algorithm the following initial parameters must be defined: types and number of atoms, charge and multiplicity, the calculation method (B3LYP, in this case) and the basis set, interatomic distances, maximum cluster volume, number of generations, size of population, and crossover and mutation rates. Most of these parameters depend on the size of the cluster. In this work, the population size was chosen to be from 15 to 20 individuals, and the GA terminates after 50 generations. This number was defined after some initial experiments and is large enough to guarantee the convergence because the global minimum is obtained within few generations. The remaining generations can help in the search for low energy isomers. The GA algorithm was used only for singlet states of clusters. For higher multiplicities, different GA runs are needed as mentioned by Alexandrova et al.[29] As our structures are small and the computational time needed to run the GA for different multiplicity is too high, we decided to run individual calculations for most of the structures that we have found with our previous GA runs. It was observed that the energies of clusters with higher multiplicities were always higher than the energies calculated for the singlet states of $(LiF)_nLi^+$. All the geometries found by the GA program were then refined using a larger 6-311+G(3df) basis set at the DFT/B3LYP level of theory.

4.2. Optimization of the Candidate Structures. Theoretical calculations have been performed, at the DFT/B3LYP/6-311+G(3df), DFT/B3LYP/LACV3P*, and MP2/LACV3P*levels, with the purpose of determining the most stable structures of the $(LiF)_nLi^+$, $(LiF)_nLi^0$, and $(LiF)_n{}^0$ series. All the calculations were carried out using the Gaussian 03[32] and Jaguar 6.0[33] software packages. The larger clusters were mainly analyzed with the Jaguar 6.0 software using the pseudospectral method to minimize the computing time.[33]

The "pool" of candidate structures (for $n \leq 4$) obtained using the GA algorithm has been used as initial structures for the refined optimization. No symmetry restrictions have been imposed in the process of geometry optimization. A vibration frequency analysis was performed for all the optimized structures at the level of calculation employed. For the reported structures all frequencies are observed to be real, indicating that the optimized structures correspond to the true minima in the respective potential energy hypersurfaces. The energy of each of the optimized structures was corrected for the zero-point energy (ZPE) to obtain the total energy (E_T = SCF + ZPE), a crucial quantity for the isomer stability analysis.

It is well-known that DFT calculations on charged species may be in error due to the fact that for most of the present available functionals the exchange energy does not exactly cancel the Coulombic self-interaction.[34] On the other hand, this effect becomes less important as the size of the ions increases. To check for possible inconsistencies, the smaller structures were also optimized at the MP2/LAVCV3P* level of calculation. No substantial changes were observed either in the geometrical parameters or in the relative stability of the clusters.

The nature of the charge distribution on the LiF clusters was investigated by calculating the atom charges for every stable structure. The atom charges were computed by fitting of the electrostatic potential using the CHelpG algorithm.[35]

4.3. *D* Plot Methodology. The *D* plot methodology was employed for a proper taxonomic description of the cluster isomers.[30,31,36,37] The *D* plot analysis takes into account about 27, 29, and 19 stable structures for the $(LiF)_nLi^+$, $(LiF)_nLi^0$, and $(LiF)_n{}^0$ series, respectively. The *D* plot is a practical method for displaying total energy differences of the distinct cluster configurations.[30,31] It consists of trying to represent the total energy of a given cluster of size n and charge q as a function of the average energy of all of the n isomers, $\langle E(n,q)\rangle$, plus a certain energy deviation, $D(n,q,i)$. Since, in general, the average energy $\langle E(n,q)\rangle$ increases linearly with n, the total energy $E_T(n)$ can be expressed as

$$E_T(n) = \langle E(n,q)\rangle + D(n,q,i) = E_0 - (E_{XY})n + D(n,q,i) \quad (1)$$

where E_0 is the total energy of the X^+ or Y^- atomic ions and the slope coefficient E_{XY} is the average total energy of the neutral XY molecule. In practice, E_0 and E_{XY} are parameters determined from the linear fit over all predicted configurations. Since $D(n,q,i) \ll E_0 - (E_{XY})_n$, these two parameters are rather insensitive to the number of configurations employed, which is not the case for $D(n,q,i)$. Lower $D_n(n,q,i)$ values correspond to lower energy isomers and thus more stable structures. The relevant features of the *D* plot are that the most stable isomers can be easily identified and the cluster families can be separated according to their trends in the *D* plot.

5. Theoretical Results and Discussion

The present study of the $(LiF)_nLi^+$, $(LiF)_nLi^0$, and $(LiF)_n{}^0$ series largely extends the theoretical results reported in ref 17, i.e., other structures for $n = 1-4$ are found, and new configurations for $n = 4-9$ are proposed. As mentioned before, up to $n < 5$ the search for structures was performed with the GA procedure, and for $n = 5-9$ the search was directed to specific clusters series. Each isomer structure is labeled as $C(n,q,i)$, where n is the cluster size (number of LiF units in the cluster), q is the cluster charge in atomic units (+1, 0, or −1) and i is the isomer index which characterizes the family type and/or the total energy: $i = 1$ for the linear structures, $i = 2$ for the planar rhombus family, $i = 3a$ for regular polygons or cyclic planar shapes ($i = 3b$ for star-shapes, not obtained for neutrals). Values of $i \geq 4$ denote tridimensional (3D) structures: $i = 4$ for cyclic parallel polygons or pyramidal shapes, $i = 5$ for cubic or cubelike structures (tending to the fcc one), and $i > 5$ for others 3D shapes (chair, spherical-like, caravel, etc.). The caravel family is characterized by a three-atom "hull" in a plane and a many-atom "sail" in a plane perpendicular to the "hull" plane.

5.1. The $(LiF)_n{}^0$, $(LiF)_nLi^0$ and $(LiF)_nLi^+$ Series. *The $(LiF)_n{}^0$ Structures.* Figure 4 shows some structures obtained for the $(LiF)_n{}^0$ clusters and classified according to the $C(n,0,i)$ notation described previously. The total energy (E_T), deviation relative to the isomeric linear structure (ΔLin), and total deviation energy ($D(n,q,i)$) values are given in Table 2. As the cluster size increases, the series structures change from planar to cubelike structures, while linear structures are observed for all the cluster sizes.

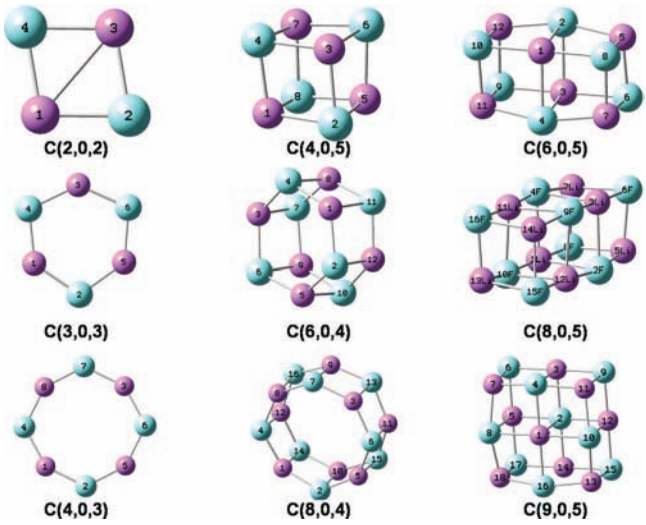

Figure 4. $C(n,0,i)$ Some predicted structures for $(LiF)_n^0$. All optimized structures are contained in the Supporting Information.

TABLE 2: Theoretical Results for the $(LiF)_n^0$ Cluster Series[a]

$C(n,0,i)$ $(LiF)_n^0$ series			DFT/B3LYP/LACV3P*				
n	i	type of structure	SCF (hartree)	ZPE (kcal/mol)	$E_T(n)$ (eV)	ΔLin (eV)	D_n (eV)
1	1	linear[21]	−107.458308	1.380	−2924.06		−0.15
2	1	linear	−214.975030	3.743	−5849.67		0.68
2	2	rhombus[21]	−215.023334	4.633	−5850.95	1.28	−0.59
3	1	linear	−322.504024	6.135	−8775.62		1.18
3	3	polygon[21]	−322.581819	7.387	−8777.68	2.06	−0.89
4	1	linear	−430.036777	8.725	−11701.65		1.58
4	3	polygon[21]	−430.128629	9.792	−11704.11	2.45	−0.88
4	5	cubelike[21]	−430.145652	11.133	−11704.51	2.86	−1.28
5	1	linear	−537.571230	11.214	−14627.74		1.93
5	6	chair	−537.688500	13.701	−14630.82	3.08	−1.16
6	1	linear	−645.106538	13.673	−17553.85		2.25
6	4	polygon 3D	−645.267932	17.088	−17558.10	4.24	−1.99
6	5	cubelike	−645.261163	16.780	−17557.93	−0.17	−1.82
7	1	linear	−752.642476	16.067	−20479.98		2.56
8	1	linear	−860.178578	18.459	−23406.12		2.86
8	4	polygon 3D	−860.376632	22.568	−23411.33	5.21	−2.35
8	5	cubelike	−860.376441	22.518	−23411.33	5.21	−2.35
9	1	linear	−967.714814	20.963	−26332.26		3.16
9	5	cubelike	−967.938930	25.268	−26338.17	5.91	−2.75

[a] D_n and ΔLin are the total deviation energy ($D_n = E_T - 2.521 + 2926.438n$) and deviation relative to the isomeric linear structure, respectively. Structures were generated using a GA (for $n < 5$) and were further optimized at the DFT/B3LYP/6-311(3df), DFT/B3LYP/LACV3P*, and MP2/LACV3P*. The configurations reported by Haketa et al.[21] are indicated. Geometry and charge distribution results are contained in the Supporting Information.

The $(LiF)_nLi^0$ Structures. Figure 5 shows some structures obtained for the $(LiF)_nLi^0$ ($n = 1-9$), identified by the same $C_{Li}(n,0,i)$ notation. Two linear $C_{Li}(1,0,1)$ structures are predicted at the DFT/B3LYP level: Li−F−Li and Li−Li−F (i = 1a); however the Li−F−Li showed one imaginary frequency at the MP2/LACV3P* level.

The Li−Li−F (i = 1a) structure is unique in the sense that no similar species were found for $n > 1$. The planar families with i = 2, 3, and 4 have a common first member (a bent Li−F−Li), but the next members differ in the way the clusters grow. For $n \geq 4$, cubelike structures are also obtained. The total energy (E_T), deviation relative to the isomeric linear structure (ΔLin), and total deviation energy ($D(n,q,i)$) values are given in Table 3.

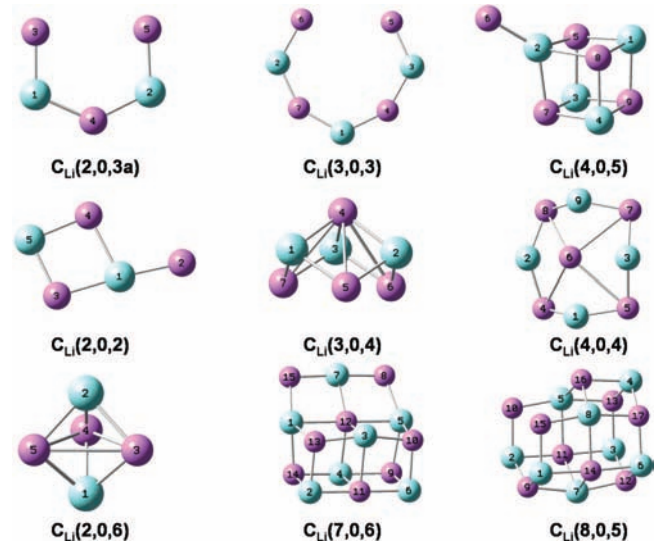

Figure 5. $C_{Li}(n,0,i)$ Some predicted structures for $(LiF)_nLi^0$. All optimized structures are contained in the Supporting Information.

The $(LiF)_nLi^+$ Structures. The shapes of the most representative structures are displayed in Figure 6 following the $C_{Li}(n,1,i)$ notation, and total energy (E_T), deviation relative to the isomeric linear structure (ΔLin), and total deviation energy ($D(n,q,i)$) values are given in Table 4. For n = 1, only the linear Li−F−Li^+ structure was found to be stable. The 2D configurations grow from a kitelike structure toward more complex kites or into rhombic structures or from a starlike structure. The 3D configurations are basically cubelike, pyramidal, caravel-like, and spherical (polyhedric-like).

5.2. *D* Plot and Clusters Stability Analysis. By use of the data presented in Tables 2−4, the values E_0 and E_{XY} can be obtained, allowing the determination of the functions $D(n,0,i)$, $D_{Li}(n,0,i)$, and $D_{Li}(n,1,i)$ for all the series studied (Figures 7). In particular, $E_{XY} \approx 2.926$ keV/LiF is found for the $(LiF)_n^0$, $(LiF)_nLi^0$, and $(LiF)_nLi^+$ structures. From the fit of the $(LiF)_nLi^+$ data one obtains E_0 = 198.695 eV, a value close to 198.09447 eV, which is the energy necessary to remove both electrons 1s from a Li^+ ion.[38]

The deviations $D(n,q,i)$ shown as a function of n in Figure 7 depend critically on the isomer i. Note that the D values are in the electronvolt range while the E_T values exceed tens of kiloelectronvolts. For example, the D plot permits to easily identify several points in Figure 7 for the $(LiF)_nLi^+$ series: (i) for the linear structures, the function D is negative up to n = 3 and then becomes positive, increasing linearly with n; (ii) for n = 2, three configurations have been found (in agreement with the results of Haketa et al.[21]): the linear structure ($C_{Li}(2,1,1)$) is more stable than the kitelike ($C_{Li}(2,1,2)$) and the diamond ($C_{Li}(2,1,6)$) structures; (iii) for n = 3, many stable structures are possible, the most stable one presenting a pyramidlike structure ($C_{Li}(3,1,4)$) with a hexagonal base and a Li^+ in the vertex followed by the linear structure; (iv) for $n \geq 4$, several structures present negative D values and become more and more stable with respect to the linear structure. In this case the polyhedral and cubelike (fcc) structures are the most stable ones.

From Tables 2−4, it is seen that for the linear structures the ZPE values vary linearly with the cluster size, n, with a slope of about 2.45 kcal/mol per LiF unit. The nonlinear structures present higher ZPE values than the corresponding linear ones.

TABLE 3: Theoretical Results for the $(LiF)_nLi^0$ Cluster Series[a]

$C_{Li}(n,0,i)$ $(LiF)_nLi^0$ series			DFT/B3LYP/LACV3P*				
n	i	type of structure	SCF (hartree)	ZPE (kcal/mol)	$E_T(n)$ (eV)	ΔLin (eV)	D_n (eV)
0		atomic Li^0	−7.491289		−203.85		
1	1a	(LiLi)F linear, 1b[21]	−114.958017	2.026	−3128.12	−1.42	1.40
1	2a	V-shape, 1a[21]	−115.013970	2.300	−3129.63	0.09	−0.11
2	3a	polygon, 2a[21]	−222.556143	5.214	−6055.90	0.31	−0.02
2	2	rhombus grid, 2b[21]	−222.557147	5.337	−6055.93	0.33	−0.04
2	6	diamond, 2c[21]	−222.541561	5.494	−6055.50	−0.10	0.39
3	4	pyramid, 3a[21]	−330.114442	8.775	−8982.59	0.89	−0.34
3	2	rhombus grid, 3b[21]	−330.106687	8.190	−8982.41	0.70	−0.16
3	3	polygon, 3c[21]	−330.101153	7.783	−8982.28	0.57	−0.03
3	6	caravel 1, 3d[21]	−330.099657	8.230	−8982.22	0.51	0.03
3	2	kite	−330.095241	7.926	−8982.11	0.40	0.14
4	1	linear	−437.616031	9.774	−11907.85		0.77
4	5	cubelike1, 4a[21]	−437.669274	11.686	−11909.22	1.37	−0.60
4	4	pyramid 1, 4b[21]	−437.660865	11.203	−11909.01	1.16	−0.39
4	2	rhombus grid, 4c[21]	−437.655556	10.957	−11908.88	1.02	−0.26
4	5	pentagon cube, 4d[21]	−437.656772	11.412	−11908.89	1.04	−0.27
4	6	chair, 4e[21]	−437.654192	11.369	−11908.82	0.97	−0.20
4	4	pyramid 2, 4g[21]	−437.646238	12.042	−11908.58	0.72	0.04
5	1	linear	−545.152635	12.210	−14834.00		0.99
5	5	cubelike 1	−545.227389	14.705	−14835.93	1.93	−0.94
5	5	cubelike 2	−545.224267	14.438	−14835.85	1.85	−0.87
6	1	linear	−652.689392	14.858	−17760.14		1.21
6	5	cubelike	−652.776908	17.686	−17762.40	2.26	−1.05
7	1	linear	−760.226129	17.019	−20686.31		1.42
7	6	chair	−760.334940	20.554	−20689.12	2.81	−1.39
7	4	star	−760.337284	20.338	−20689.19	2.88	−1.46
8	1	linear	−867.762916	19.470	−23612.46		1.63
8	5	cubelike	−867.911398	23.648	−23616.32	3.86	−2.23
8	2	kite	−867.806943	21.173	−23613.58	1.12	0.51
9	1	linear	−975.299780	21.827	−26538.62		1.84

[a] D_n and ΔLin are the total deviation energy ($D_n = E_T + 203.145 + 2926.369n$) and deviation relative to the isomeric linear structure, respectively. Structures were generated using a GA (for $n < 5$) and were further optimized at the DFT/B3LYP/6-311(3df), DFT/B3LYP/LACV3P*, and MP2/LACV3P*. The configurations reported by Haketa et al.[21] are indicated. Optimized geometries, atomic charge distributions, and MP2 results ($n < 6$) are contained in the Supporting Information.

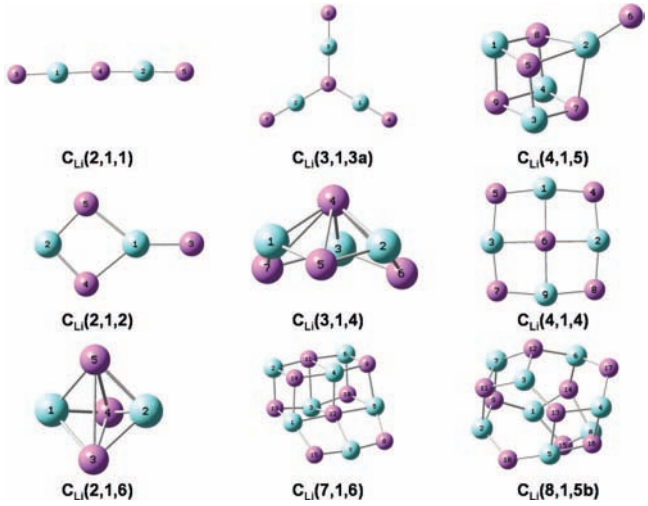

Figure 6. $C_{Li}(n,1,i)$ Some predicted structures for $(LiF)_nLi^+$. All optimized structures are contained in the Supporting Information.

For a given n, whenever a cubic structure is possible, it presents the highest ZPE value.

An attempt at understanding the relative stabilities of the clusters can be made based on their structures and charge distributions. Atomic charges, for all the reported structures, obtained from the integration of the electrostatic potential using the ChelpG algorithm[35] as well as the respective optimized geometries are contained in the Supporting Information.

For the neutral $(LiF)_n^0$ series, since only one covalent but highly polar bond can be formed between the Li and F atoms, the LiF units of the cluster will be held together mainly by dipole−dipole type interactions which vary as $(1/r^3)$ where r is the distance between the dipoles. For the linear structures, as the chain length increases the average distance between the LiF units increases while their dipoles do not change appreciably. Therefore, one should expect a decrease in the stability of the clusters with increasing the chain length as shown in the D plot (Figure 7). For the polygonal structures, the dipole moment of the LiF units is identical to that of the single unit and the units are closer to each other than in the respective linear isomers. Thus, one should expect the polygonal planar structures to be more stable than the corresponding linear ones as observed in Figure 7 and Table 2. On the other hand, as the number of units of the polygonal planar clusters increases, the distance between the LiF units also increases, leading to a stability decrease that sets a limit to single ring planar structures ($C(n,0,3)$), as shown in Table 2. The same sort of reasoning can be used to analyze the relative stability of the 3D cyclic and cubic structures. Quite interestingly, as the number of rings of the 3D cyclic structures increases, the number of first F neighbor atoms to a Li atom (or vice versa) and the average distance among them may become similar to these properties in the traditional rocky salt cubic structure. Thus, for $n > 6$, the 3D cyclic structures may become even more stable than the cubic ones (Figure 7a).

For the neutral $(LiF)_nF^0$ linear clusters the atomic charge distribution is symmetric relative to the central F (n odd) or Li (n even) atom and decreases, in absolute value, from the central atom to both ends of the chain. Thus, the clusters can be viewed as being formed from LiF units symmetrically displaced relative

TABLE 4: Theoretical Results for the $(LiF)_nLi^+$ Cluster Series[a]

$C_{Li}(n,+1,i)$ $(LiF)_nLi^+$ series			DFT/B3LYP/LACV3P*				
n	i	type of structure	SCF (hartree)	ZPE (kcal/mol)	$E_T(n)$ (eV)	ΔLin (eV)	D_n (eV)
0		atomic Li^+	−7.284906		−198.23		
1	1	linear, 1a+[21]	−114.859907	2.330	−3125.43		−0.23
2	1	linear, 2a+[21]	−222.408843	4.891	−6051.91		−0.20
2	2	kite, 2b+[21]	−222.394902	5.321	−6051.51	−0.40	0.20
2	6	diamond, 2c+[21]	−222.386942	5.629	−6051.28	−0.63	0.43
3	1	linear, 3c+[21]	−329.951163	7.373	−8978.21		0.00
3	4	pyramid, 3a+[21]	−329.972033	8.956	−8978.71	0.50	−0.50
3	3	kite	−329.949298	7.876	−8978.14	−0.07	0.08
3	2	rhombus grid, 3b+[21]	−329.947944	8.210	−8978.09	−0.12	0.13
3	7	kite diamond 1	−329.942175	8.402	−8977.92	−0.29	0.29
3	7	kite diamond 2	−329.934495	8.022	−8977.73	−0.48	0.49
3	3a	star	−329.921442	7.381	−8977.40	−0.81	0.81
3	6	diamond	−329.918804	7.768	−8977.31	−0.90	0.90
4	1	linear	−437.491036	9.812	−11904.45		0.27
4	5	cubelike, 4a+[21]	−437.507440	11.333	−11904.83	0.38	−0.11
4	2	grid, 4b+[21]	−437.542774	11.571	−11905.78	1.33	−1.06
5	1	linear	−545.029830	12.170	−14830.66		0.57
5	5b	kite	−545.088075	14.735	−14832.13	1.47	−0.90
5	5	cube	−545.086453	14.673	−14832.09	1.43	−0.86
6	1	linear	−652.567999	14.662	−17756.85		0.89
6	7	spherical	−652.658769	17.973	−17759.18	2.33	−1.44
7	1	linear	−760.105803	17.093	−20683.03		1.21
7	6	chair	−760.216781	20.565	−20685.90	2.87	−1.65
7	5b	spherical	−760.212553	20.743	−20685.78	2.75	−1.53
8	1	linear	−867.643401	19.521	−23609.21		1.55
8	5b	spherical	−867.770828	23.650	−23612.49	3.29	−1.74
8	3	kite	−867.684884	21.362	−23610.25	1.05	0.50
9	1	linear	−975.180880	21.896	−26535.38		1.88

[a] D_n and ΔLin are the total deviation energy ($D_n = E_T + 198.695 + 2926.507n$) and deviation relative to the isomeric linear structure, respectively. Structures were generated using a GA (for $n < 5$) and were further optimized at the DFT/B3LYP/6-311(3df), DFT/B3LYP/LACV3P*, and MP2/LACV3P*. The configurations reported by Haketa et al.[21] are indicated. Optimized geometries, atomic charge distributions, and MP2 results ($n < 7$) are contained in the Supporting Information.

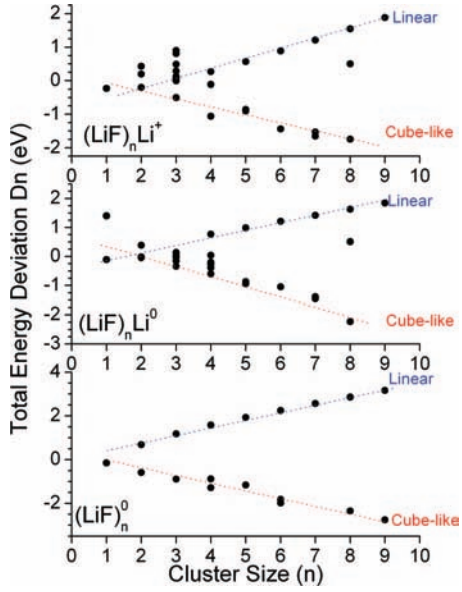

Figure 7. D plots for the $(LiF)_n^0$, $(LiF)_nLi^0$, and $(LiF)_nLi^+$ cluster series.

to the central Li atom (n odd) or to a central (Li−F−Li) unit for n even. The atomic charges in the LiF units are practically the same for all clusters and depend only on the position of the unit relative to the center of the chain (see Supporting Information). For this type of cluster, besides the dipole−dipole type interactions, for n even the cluster can be also stabilized by dipole-monopole interactions with the central charged Li atom, which vary as (q/r^2), where q is the charge of the ion. Because of the symmetric atomic charge distribution, for n odd, the dipole moment of the central (Li−F−Li) unit vanishes but not its charge. Thus, the interaction of the LiF units with the central (Li−F−Li) could be approximately described as a dipole−monopole interaction with the net charge of the central unit on the F atom. However, because of the extra dipole−monopole stabilization, the decrease in stability due to the chain length increase is not as pronounced as for $(LiF)_nLi^0$ clusters when compared to the $(LiF)_n^0$ ones (Figure 7). The cyclic planar structures for the $(LiF)_nLi^0$ clusters are not stable because in order to form this type of structure one has to bring two positively charged Li atoms close together. For the same reason one should expect mainly nonregular 3D stable structures.

The linear $(LiF)_nLi^+$ clusters also show a symmetric atomic charge distribution relative to the central F (n odd) or Li (n even). However, differently from the neutral $(LiF)_nLi^0$ clusters, the atomic charges on the Li−F units remain practically the same [Li(+0.93) F(−0.92)] independently of the distance from the central atom. Besides that, as the chain length increases the charge on the central Li atom or the net charge on the central (Li−F−Li) unit decreases and the stabilization due to ion−dipole interactions is reduced. The dipole−dipole interactions will also be less effective than in the neutral clusters because in the latter ones the LiF units with larger dipole moments are closer to each other. Hence, relative to the neutral clusters, one should expect a more pronounced decrease in stability as the chain length increases as observed in Figure 7. As for the neutral ones (e.g., LiF_n^0), large cyclic planar structures ($n > 5$) are not stable and only nonregular planar structures as well as 3D structures can be formed.

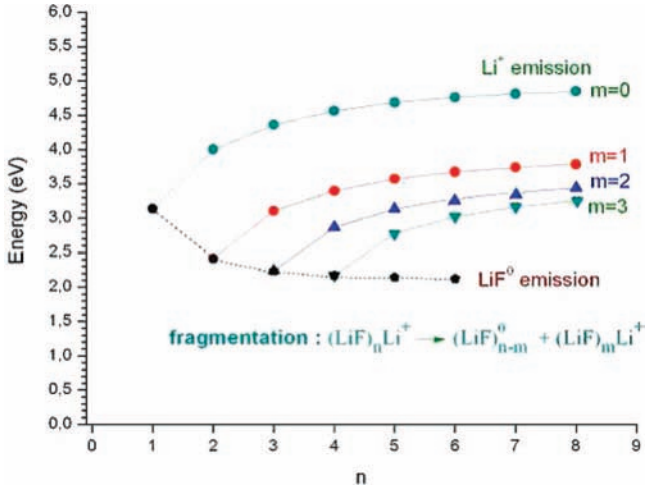

Figure 8. Fragmentation energy dependence on the cluster size for the linear $(LiF)_nLi^+$ series. FE(n,m) is the energy for the $(LiF)_nLi^+$ fragmentation into $(LiF)_{n-m}{}^0$ and $(LiF)_mLi^+$. The dashed line corresponds to $n - m = 1$, i.e., for neutral LiF detachment.

5.3. Fragmentation Energies. The fragmentation energies, $FE_{LiF}(n,m)$, can be calculated for all isomers as a function of the cluster size, n, from the total energies E_T presented in Tables 2−4. The fragmentation energies of the $(LiF)_nLi^+$ cluster are given by

$$FE_{LiF}(n,m) = E_T[(LiF)_mLi^+)] + E_T[(LiF)_{n-m}] - E_T[(LiF)_nLi^+)] \quad (2)$$

For $n - m = 1$, $FE_{LiF}(n,m)$ also defines the binding energy $BE_{LiF}(n,m)$ of the cluster. As an illustration, the results obtained for the linear structures are presented in Figure 8. The main characteristics can be summarized in:

(i) as n increases, the production of LiF^0 upon fragmentation is favored relative to that of Li^+. This is probably related to the fact that in the $(LiF)_nLi^+$ linear clusters the net charge in the units at the ends of the chain are large, which makes charge redistribution energetically easier for the emission of neutral species;

(ii) the FE(n,m) data suggest that the larger linear ion clusters decay preferentially by successive loss of LiF units.

5.4. Analysis of the PDMS-TOF Spectrum. A complete analysis of the experimental spectrum would require a detailed description of the dynamics of formation and fragmentation of all the ions, a task presently impossible to be accomplished. However, if one considers that the time scale of the TOF measurements (10^{-7} s in the acceleration region and $\sim 10^{-6}$ s in the free field region) is much larger than the time elapsed since the ionic clusters formation, reorganization and fragmentation ($\sim 10^{-14}-10^{-13}$ s), it is quite reasonable to assume that the species being detected (which are the ones emitted with low excitation energy or formed during the time interval of $\sim 10^{-8}-10^{-7}$ s) are thermodynamically more stable. Hence, one could try to relate the relative yields in the TOF spectrum to the relative stability of the clusters and their fragmentation pattern. However, even under this assumption only a tentative analysis can be advanced inasmuch as one cannot claim that all isomers for a given value of n have been found in spite of the extensive search performed. Of course, one must also take into account the process by which the clusters have been produced. Since they have been generated by high energy ^{252}Cf fission fragment collisions with the LiF target, it is reasonable to assume that the clusters should contain an excess of internal vibration (and rotation) energy that could be used to break the larger clusters into smaller and more stable clusters before detection takes place.

Overall, the spectrum of desorbed positive ions shows basically three cluster ion series: a dominant $(LiF)_nLi^+$ series, a relatively low-yield $(LiF)_n{}^+$ series, and a $Li_n{}^+$ series presenting desorption yields that decrease very fast as n increases. The yield for the dominant $(LiF)_nLi^+$ series decreases roughly as $\exp(-kn)$, where $k \approx 0.9$ for $n = 0-3$ and $k \approx 0.6$ for the heavier clusters ($n = 4-9$) while the yield of the $(LiF)_n{}^+$ series also decreases exponentially as n increases with k $\sim$ 0.6. The very fast decrease with increasing n exhibited by the $Li_n{}^+$ series is easy to understand even if no calculations have been presented for this series. The first member of this series, the $Li_2{}^+$ molecule, is already weakly bound ($D_0 = 1.4$ eV)[39,40] and the addition of another Li atom will lead preferentially to an isosceles triangular $Li_3{}^+$ structure corresponding either to a neutral Li_2 molecule interacting with a Li^+ ion or to a $Li_2{}^+$ molecule interacting with a neutral Li atom. Since the bond energy of the Li_2 molecule is smaller ($D_0 = 1.04$ eV)[39] than that of $Li_2{}^+$, the second member of this series will most probably correspond to the $Li_2{}^+-Li$ system but with the $Li_2{}^+$ unit less strongly bonded. As n increases, an even weaker bonded $Li_2{}^+$ unit interacts with weakly bonded Li_2 units, and therefore one should expect an increase in instability as n increases, in agreement with the experimental observation.

The analysis of the $(LiF)_n{}^+$ series is quite speculative because no calculations have been performed for the members of this series and a large variety of geometries can in principle be adopted by the clusters as n increases. However, in this case the Li−F bond energy in the neutral molecule is quite large ($D_0 = 5.91$ eV).[39] Also, the bond energy of the $(LiF)^+$ species should not be very different from that of the neutral one because this species is formed from the neutral one by removing one electron from a nonbonding orbital. Thus, the larger clusters should be held together by electrostatic forces among strong covalent species. That is, any excess of internal vibration energy would favor the decomposition of larger cluster into the smaller more stable ones, since the covalent forces would be stronger than the electrostatic ones holding the units together.

For the linear $(LiF)_nLi^+$ series the fragmentation energies are smaller for the channel producing LiF neutral units. Also, the fragmentation energies for that channel decrease faster for $1 \leq n \leq 3$ and much slower for $n \geq 4$. If one assumes that all types of clusters in this series exhibit the same fragmentation pattern, it is possible to understand the abundances in the spetcrum as well as the fact that two exponential functions ($k \approx 0.9$ for $n = 1-3$, faster decay; $k \approx 0.6$ for $n = 4-9$, slower decay) are needed to fit the abundances of the smaller and larger clusters.

6. Conclusions

Experimental data of desorbed positive ions from polycrystalline LiF bombarded by $\sim$60 MeV ^{252}Cf fission fragments show basically three cluster ion series: a dominant $(LiF)_nLi^+$ series, a relatively low yield $(LiF)_n{}^+$ series, and a $Li_n{}^+$ series presenting desorption yields that decrease very fast as n increases. The intense secondary emission of Li^+ ions and $(LiF)_nLi^+$ clusters (particularly the $LiFLi^+$ species) is expected since they are abundant debris of the solid target. On the contrary, emission of $(LiF)_n{}^+$ ions should be disfavored with respect to other natural debris, the $(LiF)_n{}^0$. The high desorption yield of Li^+ combined with the very low yields of $(Li)_2{}^+$ and $(Li)_3{}^+$ indicate that the reaction $Li^+ + Li^0 \rightarrow Li_2{}^+$ is a relatively rare event, possibly due to a low concentration of Li^0 in the plasma after impact.

DFT and MP2 calculations of the clusters geometries and fragmentation energies have been performed as an effort for determining the cluster structures and for understanding the observed cluster ion abundances. The $(LiF)_n^0$, $(LiF)_nLi^0$, and $(LiF)_nLi^+$ configurations reported in this work largely extend the previous results obtained by Hareta et al.,[21] Aguado et al.,[20] and Bichoutskaia et al.[15] On the basis of the predicted total energy, the obtained structures are classified in different families. It is concluded that linear structures are very stable for small $(LiF)_nLi^+$ cluster ions ($n = 1-3$), while symmetric and closed packed structures (particularly the polyhedron-like and fcc-like) are more stable for large cluster sizes ($n = 4-9$). The most stable $(LiF)_n^0$ clusters are not linear but rather they exhibit cubic or polygonlike structures.

The fragmentation energy dependence on the size of the cluster was determined for the linear structures. Because of the lower FE values for LiF^0 emission with respect to Li^+ emission, it is suggested that the bombarded LiF solid or a desorbed excited $(LiF)_nLi^+$ cluster dissociates via a cascade of $(LiF)_n^0$ units. By assumption that the clusters of the $(LiF)_nLi^+$ series exhibit the same fragmentation pattern, it is possible to understand the relative $(LiF)_nLi^+$ population distribution observed in the experiment as well as the fact that two exponential functions ($k \approx 0.9$ for $n = 1-3$, faster decay; $k \approx 0.6$ for $n = 4-9$, slower decay) are needed to fit the abundances of the smaller and larger clusters.

Acknowledgment. The authors acknowledge the Brazilian Agencies CNPq and FAPERJ for partial support.

Supporting Information Available: This material is available free of charge via the Internet at http://pubs.acs.org.

References and Notes

(1) Ytoh, N. *Nuc. Instrum. Meth.* **1987**, *B 27*, 155.
(2) Szymonski, M. *Mat.-Fys. Medd.* **1993**, *43*, 495.
(3) Pereira, J.A. M.; de Castro, C. S. C.; Jeronymo, J. M. F.; Ponciano, C. R.; da Silveira, E. F.; Wien, K. *Instrum. Meth.* **1997**, *B 129*, 21.
(4) Pereira, J.A. M.; da Silveira, E. F.; Wien, K. *Radiat. Effects Defects Solids* **1997**, *142*, 247.
(5) Pereira, J.A. M.; da Silveira, E. F. *Phys. Rev. Lett.* **2000**, *84*, 5904.
(6) *Alkali Halides: A handbook of Physical Properties*; Sirdeshmukh, B., ED.; Springer, 2001; p 6.
(7) Fernández-Lima, F. A.; Ponciano, C. R.; da Silveira, E. F. *J. Mass Spectrom.* **2008**, *43*, 587.
(8) Ponciano, C. R.; Ávalos, F. E.; Rentería, A.; da Silveira, E. F. *Int. J. Mass Spectrom.* **2001**, *209*, 197.
(9) Ponciano, C. R.; Martinez, R.; da Silveira, E. F. *J. Mass Spectrom.* **2007**, *42*, 1300.
(10) Roy, L. *Johnston, Atomic and Molecular Cluster, Master Series in Physics and Astronomy*; Betts, D.S.; London and New York, 2002.
(11) Martin, T. P. *Phys. Rep.* **1996**, *273*, 199.
(12) Yokoyama, K.; Haketa, N.; Hashimoto, M.; Furukawa, K.; Tanaka, H.; Kudo, H. *Chem. Phys. Lett.* **2000**, *320*, 645.
(13) Jalowy, T.; Farenzena, L. S.; Ponciano, C. R.; Schmidt-Böcking, H.; da Silveira, E. F.; Groeneveld, K. O. *Surf. Sci.* **2004**, *557*, 91.
(14) Pereira, J. A. M.; Bitensky, I. S.; da Silveira, E. F. *Phys. Res. B* **1998**, *135*, 244.
(15) Bichoutskaia, E.; Pyper, N. C. *Chem. Phys. Lett.* **2006**, *423*, 234.
(16) Pearson, P. K.; Hunt, W. J.; Bender, C. F.; Schaefer, H. F., III. *J. Chem. Phys.* **1973**, *58*, 5358.
(17) Gutowski, M.; Simons, J. *J. Chem. Phys.* **1994**, *100*, 1308.
(18) Kunz, A. B. *Phys. Rev.* **1982**, *26*, 2056.
(19) Pandey, R.; Seel, M.; Kunz, A. B. *Phys. Rev.* **1990**, *B 41*, 7955.
(20) Aguado, A.; Alonso, J. A. *Phys. Rev.* **1997**, *B 56*, 15353.
(21) Haketa, N.; Yokoyama, K.; Tanaka, H.; Kudo, H. *THEOCHEM* **2002**, *B 577*, 55.
(22) Michalewicz. Z. *Genetic Algorithms + Data Structures = Evolution Programs*; Springer-Verlag; 1996.
(23) Zebulum, R. S.; Pacheco, M. A. C.; Maria, M.; Vellasco; B. R. *Evolutionary Electronics: Automatic Design of Electronic Circuits and Systems by Genetic Algorithms*; CRC Press: Boca Raton, FL, 2001.
(24) Hartke, B. *J. Phys. Chem.* **1993**, *97*, 9973.
(25) Xiao, Y.; Williams, D. E. *Chem. Phys. Lett.* **1993**, *215*, 17.
(26) Zeiri, Y. *Phys. Rev. E* **1995**, *51*, 2769.
(27) Deaven, D. M.; Ho, K. M. *Phys. Rev. Lett.* **1995**, *75*, 288.
(28) Alexandrova, A. N.; Boldyrev, A. I. *J. Chem. Theory Comput.* **2005**, *1*, 566.
(29) Alexandrova, A. N.; Boldyrev, A. I.; Fu, Y. J.; Yang, X.; Wang, X. B.; Wang, L. S. *J. Chem. Phys.* **2004**, *121*, 5709.
(30) Fernandez-Lima, F. A.; Ponciano, C. R.; Nascimento, M. A. C.; da Silveira, E. F. *Chem. Phys. Lett.* **2006**, *426*, 351.
(31) Fernandez-Lima, F. A.; Ponciano, C. R.; Faraudo, G. S.; Grivet, M.; da Silveira, E. F.; Nascimento, M. A. C. *Chem. Phys.* **2007**, *340*, 127.
(32) Frisch, M. J.; Trucks, G. W.; Schlegel, H. B.; Scuseria, G. E.; Robb, M. A.; Cheeseman, J. R.; Montgomery, J. A., Jr.; Vreven, T.; Kudin, K. N.; Burant, J. C.; Millam, J. M.; Iyengar, S. S.; Tomasi, J.; Barone, V.; Mennucci, B.; Cossi, M.; Scalmani, G.; Rega, N.; Petersson, G. A.; Nakatsuji, H.; Hada, M.; Ehara, M.; Toyota, K.; Fukuda, R.; Hasegawa, J.; Ishida, M.; Nakajima, T.; Honda, Y.; Kitao, O.; Nakai, H.; Klene, M.; Li, X.; Knox, J. E.; Hratchian, H. P.; Cross, J. B.; Bakken, V.; Adamo, C.; Jaramillo, J.; Gomperts, R.; Stratmann, R. E.; Yazyev, O.; Austin, A. J.; Cammi, R.; Pomelli, C.; Ochterski, J. W.; Ayala, P. Y.; Morokuma, K.; Voth, G. A.; Salvador, P.; Dannenberg, J. J.; Zakrzewski, V. G.; Dapprich, S.; Daniels, A. D.; Strain, M. C.; Farkas, O.; Malick, D. K.; Rabuck, A. D.; Raghavachari, K.; Foresman, J. B.; Ortiz, J. V.; Cui, Q.; Baboul, A. G.; Clifford, S.; Cioslowski, J.; Stefanov, B. B.; Liu, G.; Liashenko, A.; Piskorz, P.; Komaromi, I.; Martin, R. L.; Fox, D. J.; Keith, T.; Al-Laham, M. A.; Peng, C. Y.; Nanayakkara, A.; Challacombe, M.; Gill, P. M. W.; Johnson, B.; Chen, W.; Wong, M. W.; Gonzalez, C.; Pople, J. A. *Gaussian 03*, revision C.02; Gaussian, Inc.: Wallingford, CT, 2004.
(33) *Jaguar 6.0*; Schrödinger Inc., Portland, OR, 2004.
(34) Fernandez-Lima, F. A.; Cardozo, T. M.; Rodriguez, R. M.; Ponciano, C. R.; da Silveira, E. F.; Nascimento, M. A. C. *J. Phys. Chem.* **2007**, *A111*, 8302.
(35) Fernandez-Lima, F. A.; Ponciano, C. R.; da Silveira, E. F.; Nascimento, M. A. C. *Chem. Phys. Lett.* **2007**, *445*, 147.
(36) Rosch, N.; Trickey, S. B. J. *Chem. Phys.* **1997**, *106*, 8940.
(37) Breneman, C. M.; Wiberg, K. W. *J. Comput. Chem.* **1990**, *11*, 361.
(38) *CRC Handbook of Chemistry and Physics*, 76th ed.; CRC Press: Boca Raton, 1996.
(39) Huber, K. P.; Herzberg, G. *Constants of Diatomic Molecules*; Van Nostrand: New York, NY, 1979.
(40) Pereira, M. S.; Nascimento, M. A. C. *Chem. Phys. Lett.* **2005**, *406*, 446.

JP8071684